

Probing Reheating with Graviton Bremsstrahlung

Nicolás Bernal,^a Simon Cléry,^b Yann Mambrini^b and Yong Xu^{1c}

^a*New York University Abu Dhabi*

PO Box 129188, Saadiyat Island, Abu Dhabi, United Arab Emirates

^b*Université Paris-Saclay, CNRS/IN2P3, IJCLab, 91405 Orsay, France*

^c*PRISMA⁺ Cluster of Excellence and Mainz Institute for Theoretical Physics
Johannes Gutenberg University, 55099 Mainz, Germany*

E-mail: nicolas.bernal@nyu.edu, clery@ijclab.in2p3.fr,
mambrini@ijclab.in2p3.fr, yonxu@uni-mainz.de

ABSTRACT: We investigate the stochastic gravitational wave (GW) spectrum resulting from graviton bremsstrahlung during inflationary reheating. We focus on an inflaton ϕ oscillating around a generic monomial potential $V(\phi) \propto \phi^n$, considering two different reheating scenarios: *i*) inflaton decay and *ii*) inflaton annihilation. We show that in the case of a quadratic potential, the scattering of the inflatons can give rise to larger GW amplitude than the decay channel. On the other hand, the GW spectrum exhibits distinct features and redshifts in each scenario, which makes it possible to distinguish them in the event of a discovery. Specifically, in the case of annihilation, the GW frequency can be shifted to values higher than those of decay, whereas the GW amplitude generated by annihilation turns out to be smaller than that in the decay case for $n \geq 4$, due to the different scaling of radiation during reheating. We also show that the differences in the GW spectrum become more prominent with increasing n . Finally, we highlight the potential of future high-frequency GW detectors to distinguish between the different reheating scenarios.

¹Corresponding author

Contents

1	Introduction	1
2	Reheating and Graviton Emission	3
2.1	Generalities	3
2.2	Graviton emission from inflaton decay	5
2.3	Graviton emission from inflaton annihilation	8
3	Gravitational Wave Spectrum	11
3.1	Overview	11
3.2	Combining graviton bremsstrahlung and reheating	14
4	Conclusions	18
A	Graviton Bremsstrahlung for a Monomial Potential	19

1 Introduction

Cosmic inflation is an elegant paradigm that solves the horizon, flatness, and monopole problems of the (old) standard cosmology [1]. A successful inflationary model must incorporate an efficient reheating mechanism to align with observational data. In the conventional scenario, after inflation, the inflaton field descends to the potential minimum, starting to oscillate and transfer energy to light degrees of freedom of the Standard Model (SM), which eventually undergo thermalization, forming the SM bath. Energy transfer can proceed through decay or annihilation of the inflaton, facilitated by the introduction of couplings between the inflaton and the daughter fields [2]. Due to the inevitable coupling between the metric and the energy-momentum tensor, the emission of graviton degrees of freedom is also anticipated through radiative bremsstrahlung processes [3, 4]. However, within the framework of general relativity, the graviton production rate is suppressed by the squared Planck mass M_P^2 , where $M_P = 1/\sqrt{8\pi G_N} \simeq 2.4 \times 10^{18}$ GeV. To achieve efficient graviton production, a high-energy scale and consequently a large energy-momentum tensor become imperative. This precise scenario unfolds during the reheating phase.

The physics that takes place during reheating is difficult to test experimentally. One of the very few observables (if not the only one) is gravitational waves (GWs). It is also known that graviton bremsstrahlung during inflationary reheating gives rise to an interesting stochastic GW background (SGWB)¹ [11–16]. The spectrum typically peaks at ultrahigh frequencies depending on the detailed dynamics of reheating, such as the shape of the inflaton potential or the inflaton-matter coupling [14, 15]. It was also recently shown

¹We notice that fluctuations in the thermal plasma could also give rise to SGWB [5–10].

that the GW spectrum can be boosted during bosonic reheating through inflaton decay, once the inflaton oscillates around the minimum of a potential steeper than quadratic, $V(\phi) \propto \phi^n$ with $n > 2$ [15]. In this case, the inflaton decay rate has a time dependence proportional to $1/\phi_0^{n-2}$ and ϕ_0^{n-2} for bosonic and fermionic reheating, respectively [17], where we have assumed that after inflation, $\phi(t) = \phi_0(t) \mathcal{P}(t)$, with $\mathcal{P}(t)$ a quasiperiodic function encoding the (an)harmonicity of short-timescale oscillations in the potential and $\phi_0(t)$ is the envelope subject to the effect of redshift and decay. Note that $\phi_0(t)$ is a decreasing function of time, leading to the radiation or entropy released in bosonic reheating being smaller compared to that during fermionic reheating. Consequently, the GW amplitude generated in bosonic reheating suffers less dilution effects, and hence tends to feature larger amplitudes.²

In the existing literature, the analysis for graviton bremsstrahlung is limited to reheating scenarios considering inflaton decays [11–16]. In this work, we generalize previous studies by including inflaton annihilation, which is also a viable reheating scenario [17–19], and compare their observational signatures in the form of GW emission. In particular, we assume that the inflaton transfers its energy predominantly to the bosonic sector, which could account for the degrees of freedom of the SM Higgs doublet.³ Although reheating is not possible through inflaton scattering for $n = 2$, SM radiation and therefore SM bath temperature feature distinct behaviors depending on the reheating channel for $n > 2$. More specifically, in the decay scenario, the temperature evolves as $T(a) \propto a^{-\frac{3}{2n+4}}$, while for annihilation $T(a) \propto a^{-\frac{9}{2n+4}}$, where a denotes the cosmic scale factor [17]. We show that the temperature dependence in the redshift is transmitted to the spectrum and amplitude of the GWs generated by the graviton-bremsstrahlung process through the dilution effect, which makes it possible to distinguish between the two reheating channels. In particular, we aim to compare the different features of the GW spectrum in inflaton decays and annihilations. This is particularly interesting because it offers the potential to utilize the GW features to pinpoint reheating scenarios with inflaton decays and annihilations. To this end, we first calculate the graviton emission rate from inflaton annihilation. Then we compute the bremsstrahlung-induced GW spectrum by solving a set of coupled Boltzmann equations.

The paper is organized as follows. In Section 2, we study the two reheating setups together with the graviton emission rates in each scenario. In Section 3, the solution for the differential GW spectrum is presented for the inflaton-annihilation scenario. Furthermore, we investigate the GW spectrum, paying particular attention to the difference between inflaton bosonic decay and annihilation. Finally, we summarize our findings in Section 4.

²Note that the GW amplitude can be written as $\Omega_{\text{GW}} \propto 1/\rho_R$, where ρ_R correspond to the energy densities stored in radiation. If ρ_R is smaller, Ω_{GW} can be larger.

³Note that for fermionic reheating, extra vector-like fermionic degree of freedoms beyond the SM of particle physics have to be introduced; in that sense, the bosonic reheating scenario is more minimal.

2 Reheating and Graviton Emission

2.1 Generalities

After inflation ends, the inflaton starts to coherently oscillate around the potential minimum, transferring its energy to the SM bath: a process called inflationary reheating [2]. The energy-transfer efficiency is controlled by the type and strength of the inflaton-matter coupling. In this paper, we focus on a bosonic reheating scenario, considering that the inflaton ϕ decays or annihilates into a real scalar φ , which could account for the degrees of freedom of the SM Higgs doublet.

The relevant interactions are described by the Lagrangian density

$$\mathcal{L} \supset \mu \phi \varphi^2 + \sigma \phi^2 \varphi^2, \quad (2.1)$$

where μ and σ are couplings with mass dimensions 1 and 0, respectively. Expanding the space-time metric $g_{\mu\nu}$ around the flat Minkowski background $g_{\mu\nu} \simeq \eta_{\mu\nu} + (2/M_P) h_{\mu\nu}$, one can write the effective coupling [20]

$$\sqrt{-g} \mathcal{L} \supset -\frac{1}{M_P} h_{\mu\nu} T^{\mu\nu}, \quad (2.2)$$

where g denotes the determinant of $g_{\mu\nu}$ and $T^{\mu\nu}$ corresponds to the energy-momentum tensor.

During reheating, we assume that the inflaton oscillates around a generic monomial potential of the form [17, 21, 22]

$$V(\phi) = \lambda M_P^4 \left(\frac{\phi}{M_P} \right)^n, \quad (2.3)$$

where λ is a dimensionless parameter. Such potential could originate, for example, from Starobinsky inflation [23], polynomial inflation [24–26] or the α -attractor inflationary T - or E -models [27, 28]. The effective mass m_ϕ of the inflaton can be defined as the second derivative of its potential and is [17, 22]

$$m_\phi(a)^2 \simeq n(n-1) \lambda^{\frac{2}{n}} M_P^{\frac{2(4-n)}{n}} \rho_\phi(a)^{\frac{n-2}{n}}, \quad (2.4)$$

which is a time-dependent quantity for $n \neq 2$ given as a function of the inflaton energy density

$$\rho_\phi = \frac{1}{2} \dot{\phi}^2 + V(\phi), \quad (2.5)$$

where dots ($\dot{}$) correspond to derivatives with respect to time.

The evolution of the energy densities for the inflaton ρ_ϕ and the SM radiation ρ_R can be tracked by the following Boltzmann equations [17, 21, 22]

$$\frac{d\rho_\phi}{dt} + 3H(1+w_\phi)\rho_\phi = -(1+w_\phi)\gamma, \quad (2.6)$$

$$\frac{d\rho_R}{dt} + 4H\rho_R = +(1+w_\phi)\gamma, \quad (2.7)$$

where $w_\phi = (n - 2)/(n + 2)$ denotes the equation of state [17, 22] and $\gamma \equiv \Gamma \rho_\phi$ is the interaction rate density for the production of SM states from inflatons. Additionally, H corresponds to the Hubble expansion rate

$$H^2 = \frac{\rho_R + \rho_\phi}{3 M_P^2}, \quad (2.8)$$

with

$$\rho_R(T) = \frac{\pi^2}{30} g_\star(T) T^4, \quad (2.9)$$

and $g_\star(T)$ being the number of relativistic degrees of freedom contributing to the SM energy density.⁴ The end of the reheating period is defined as the moment at which the SM radiation starts to dominate the total energy density of the universe and corresponds to a reheating temperature T_{RH} (or equivalently, a scale factor $a_{\text{RH}} \equiv a(T_{\text{RH}})$) given by $\rho_R(T_{\text{RH}}) = \rho_\phi(T_{\text{RH}}) = 3 M_P^2 H_{\text{RH}}^2$, where $H_{\text{RH}} \equiv H(T_{\text{RH}})$.

During reheating, that is, when $\Gamma \ll H$, Eq. (2.6) admits an approximate analytical solution given by

$$\rho_\phi(a) \simeq \rho_\phi(a_{\text{RH}}) \left(\frac{a_{\text{RH}}}{a} \right)^{\frac{6n}{n+2}}, \quad (2.10)$$

and therefore, the effective inflaton mass can be rewritten as

$$m_\phi(a) = m_\phi^{\text{RH}} \left(\frac{a_{\text{RH}}}{a} \right)^{\frac{3(n-2)}{n+2}}, \quad (2.11)$$

with

$$m_\phi^{\text{RH}} \equiv m_\phi(a_{\text{RH}}) \simeq \sqrt{n(n-1)} \lambda^{\frac{1}{n}} M_P \left(\sqrt{3} \frac{H_{\text{RH}}}{M_P} \right)^{\frac{n-2}{n}}. \quad (2.12)$$

Depending on the form of γ , the solution for $\rho_R(a)$ and therefore the temperature $T(a)$ during reheating exhibits distinct characteristics, which would consequently give rise to different dilution effects for the generated GW spectrum. In the following sections, we will present the scenarios with inflaton bosonic decay and annihilation.

However, before proceeding, it is important to comment on several points. We have assumed that the effects of non-perturbative preheating [32, 33], inflaton fragmentation [34–36], and gravitational reheating [37–41] are subdominant compared to perturbative decay. Note that even if non-perturbative phenomena during reheating could lead to the equation of state approaching 1/3 during reheating, perturbative decay is still necessary to fully deplete the inflaton energy [42, 43]. Furthermore, for the bosonic decay scenario, the inefficiency of preheating has been highlighted as the result of self-interaction of the generated daughter field [42]. In particular, the trilinear coupling $\mu \phi \varphi^2$ gives rise to a tachyonic squared mass $m_\varphi^2 \sim \mu \phi$ for the field φ once ϕ crosses zero and becomes negative. However, the self-interaction of the φ fields $\lambda_\varphi \varphi^4$ gives rise to a positive squared mass term $m_\varphi^2 \sim \lambda_\varphi \langle \varphi^2 \rangle$ where $\langle \varphi^2 \rangle$ corresponds to the variance of φ . This backreaction counteracts tachyonic effects and quickly terminates preheating, making it inefficient [42]. Additionally,

⁴Note that during our study, we assumed instantaneous thermalization, for details of the effects of non-instantaneous thermalization, see Refs. [29–31].

when the inflaton features self-interactions or, equivalently, when the inflaton potential is steeper than quadratic, the effects of inflaton fragmentation are relevant. Indeed, in the case of decays into fermions, fragmentation is particularly important, making perturbative decays subdominant [36]. However, in the case of decay or scattering of the inflaton to scalars, the effect is milder.

Lastly, to be dominant, the gravitational reheating mechanism requires $w_\phi \gtrsim 0.65$, corresponding to $n > 9$ [38, 39, 44, 45]. This bound can be relaxed to $n > 4$ if one introduces a non-minimal coupling between gravity and a pair of inflatons [46], or even to $n \geq 2$ if gravity couples non-minimally to a single inflaton [40]. In the current work, we focus on scenarios with $2 \leq n \leq 6$ minimally coupled to gravity with high-temperature reheating, where the effects of inflaton fragmentation and gravitational reheating are expected to be subdominant.

2.2 Graviton emission from inflaton decay

In this section, we briefly review the case of inflaton bosonic decays [14, 15]. The rate of inflaton decay into a pair of real scalars φ with mass m is given by

$$\Gamma^{1 \rightarrow 2} \simeq \frac{m_\phi}{8\pi} \left(\frac{\mu_{\text{eff}}}{m_\phi} \right)^2, \quad (2.13)$$

where

$$\mu_{\text{eff}}^2(n) \simeq (n+2)(n-1) \mu^2 \frac{\varpi}{m_\phi} \sum_{j=1}^{\infty} j |\mathcal{P}_j|^2 \left\langle \left(1 - \frac{4y^2}{j^2} \mathcal{P} \right)^{1/2} \right\rangle \quad (2.14)$$

corresponds to the effective coupling after averaging over inflaton oscillations [17], and $y \equiv m/\varpi$. We introduced the Fourier decomposition of the oscillating field

$$\phi(t) = \phi_0(t) \mathcal{P}(t) = \phi_0(t) \sum_{j=1}^{\infty} \mathcal{P}_j(t) e^{-ij\varpi t}. \quad (2.15)$$

The j^{th} oscillating mode is associated with an energy $E_j = j\varpi$ where ϖ is the frequency of the oscillating background field. It is a time-dependent quantity related to the effective inflaton mass and amplitude via

$$\varpi = \sqrt{\frac{n\pi}{2(n-1)}} \frac{\Gamma(\frac{1}{2} + \frac{1}{n})}{\Gamma(\frac{1}{n})} m_\phi = \alpha_n \sqrt{\lambda} M_P \left(\frac{\phi_0}{M_P} \right)^{\frac{n-2}{2}}. \quad (2.16)$$

We note that the energy in each mode is time dependent for $n > 2$ and that each mode contributes to the production rate, as can be seen from the sum in the expression above. In what follows, we neglect the contribution of higher-order modes $j > 1$ and look at the leading contribution $j = 1$.

In the case of decays, the rate density $\gamma = \rho_\phi \Gamma^{1 \rightarrow 2}$, and therefore Eq. (2.7) admits the analytical solution [47]

$$\rho_R(a) \simeq \frac{n}{1+2n} \rho_\phi(a_{\text{end}}) \left(\frac{a_{\text{end}}}{a} \right)^{\frac{6}{n+2}} \left[1 - \left(\frac{a_{\text{end}}}{a} \right)^{\frac{2+4n}{2+n}} \right] \left(\frac{a_{\text{end}}}{a_{\text{RH}}} \right)^{\frac{6(n-1)}{2+n}}, \quad (2.17)$$

where a_{end} and a_{RH} denote the scale factor at the end of inflation and of reheating, respectively, which implies that during reheating

$$T(a) = T_{\text{RH}} \left(\frac{a_{\text{RH}}}{a} \right)^\alpha, \quad (2.18)$$

with

$$\alpha \equiv \frac{3}{2n + 4}. \quad (2.19)$$

It is important to note that away from the instantaneous decay approximation of the inflaton, the SM bath could reach temperatures higher than T_{RH} , up to T_{max} [48]. This can be observed in Fig. 1, where we show the evolution of the energy densities of the inflaton and SM radiation (left) and the temperature of the SM bath (right) as a function of the scale factor for the cases of inflaton annihilations and decays. Reheating occurs in the range $a_{\text{end}} < a < a_{\text{RH}}$. Earlier times correspond to the cosmic inflationary epoch, while later times to the SM radiation-dominated isentropic era, where $T(a) \propto a^{-1}$. We note that to solve Eqs. (2.6) and (2.7), one has to fix the interaction rate density γ of the inflaton (and, therefore, its mass and couplings to the daughter particles), its initial energy density $\rho_\phi(a_{\text{end}})$ and n . We recall that at the end of inflation $\rho_R(a_{\text{end}}) = 0$ is expected. However, it is more convenient to choose, instead of γ and $\rho_\phi(a_{\text{end}})$ as free parameters, T_{RH} and T_{max} . The latter set of parameters is used in the following analysis. In the upper panels of Fig. 1, we have chosen $n = 4$, $T_{\text{RH}} = 10^{13}$ GeV with $T_{\text{max}} = 3.6 \times 10^{13}$ GeV, while in the lower panels $n = 6$, $T_{\text{RH}} = 10^{13}$ GeV with $T_{\text{max}} = 2.4 \times 10^{13}$ GeV. We consider T_{RH} as a free parameter and then compute T_{max} in the α -attractor T -model considering the central values of the amplitude of the primordial spectrum of curvature perturbations and its associated spectral tilt: $n_s = 0.9659$ and $A_s = 2.1 \times 10^{-9}$ [49].

In addition to the 2-body decay, there is an inexorably associated graviton emission by bremsstrahlung, as shown in Fig. 2. It is interesting to note that from the four possible diagrams, two of the matrix elements (the first and the last) vanish because the inflaton decays with vanishing three momenta and the graviton polarization tensor is traceless [14]. The differential decay width for the inflaton condensate with respect to the graviton energy E_ω for this 3-body decay process is given by [17]

$$\frac{d\Gamma^{1 \rightarrow 3}}{dE_\omega} = \frac{m_\phi}{\rho_\phi(1 + w_\phi)} \sum_{j=1}^{\infty} \int |\mathcal{M}_j^{1 \rightarrow 3}|^2 \frac{d\text{PS}^{(3)}}{dE_\omega}, \quad (2.20)$$

where $d\text{PS}^{(3)}$ is the 3-body Lorentz-invariant phase space, leading to⁵

$$\frac{d\Gamma^{1 \rightarrow 3}}{dE_\omega} \simeq \frac{1}{16\pi^3} \left(\frac{\mu_{\text{eff}}}{M_P} \right)^2 \left[\frac{(1 - 2x)(1 - 2x + 2y^2)}{4x\zeta^{-1}} + \frac{y^2(y^2 + 2x - 1)}{x} \ln \left(\frac{1 + \zeta}{1 - \zeta} \right) \right], \quad (2.21)$$

with $x \equiv E_\omega/\varpi$, and

$$\zeta \equiv \sqrt{1 - \frac{4y^2}{1 - 2x}}. \quad (2.22)$$

⁵Note that this is consistent with the result presented in Ref. [14] where it was assumed that the final state contains different particles and that there are two decay channels. The prefactor in Ref. [14] is 1/32, which recovers to 1/16 after multiplying $2^2/2$.

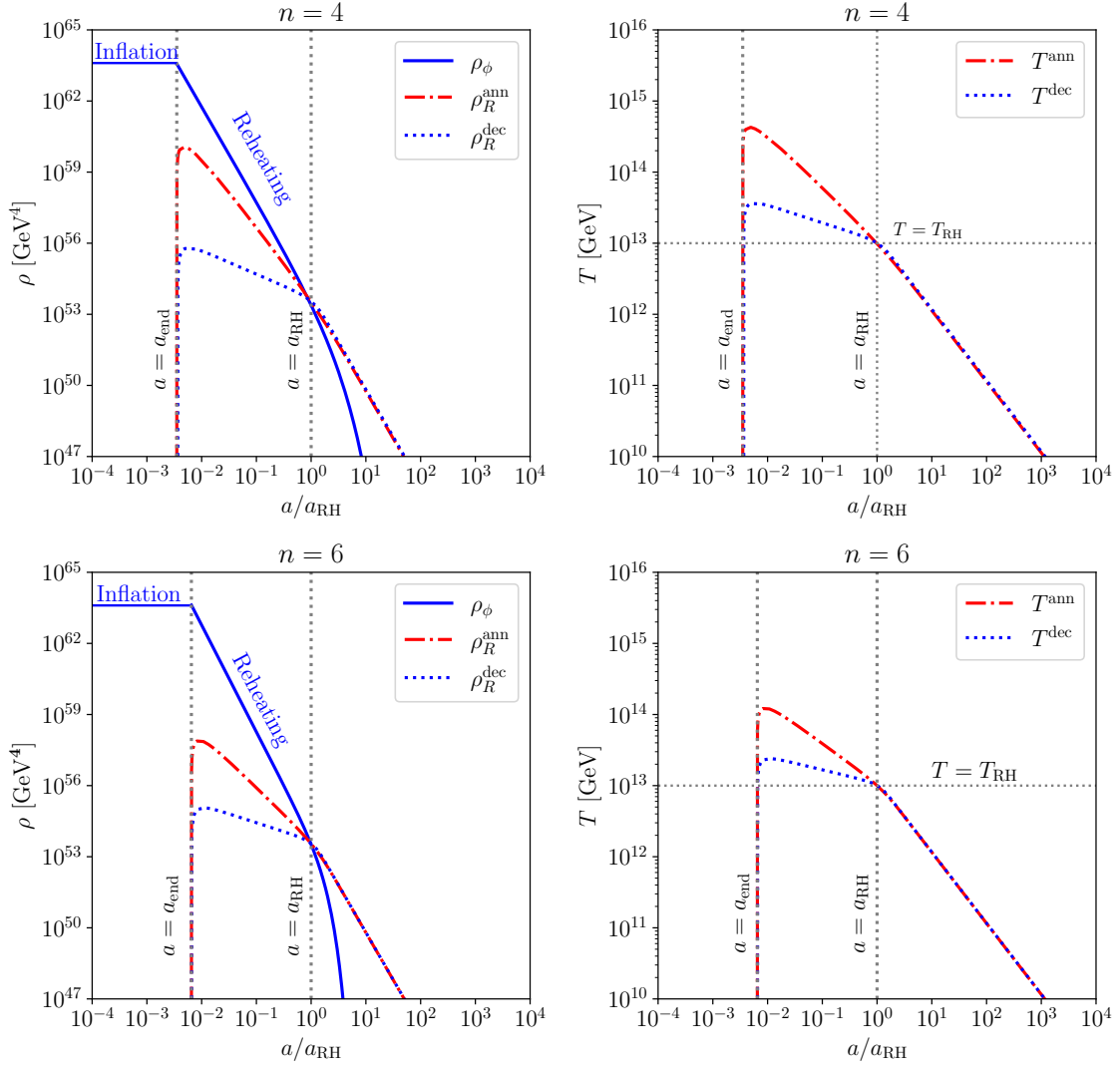


Figure 1. Evolution for energy densities (left) and temperature (right), for $T_{\text{RH}} = 10^{13}$ GeV. In the upper panels, we have chosen $n = 4$ and $T_{\text{max}} = 3.6 \times 10^{13}$ GeV for decays ($T_{\text{max}} = 4.3 \times 10^{14}$ GeV for annihilations), while in the lower panels $n = 6$ and $T_{\text{max}} = 2.4 \times 10^{13}$ GeV for decays ($T_{\text{max}} = 1.2 \times 10^{14}$ GeV for annihilations).

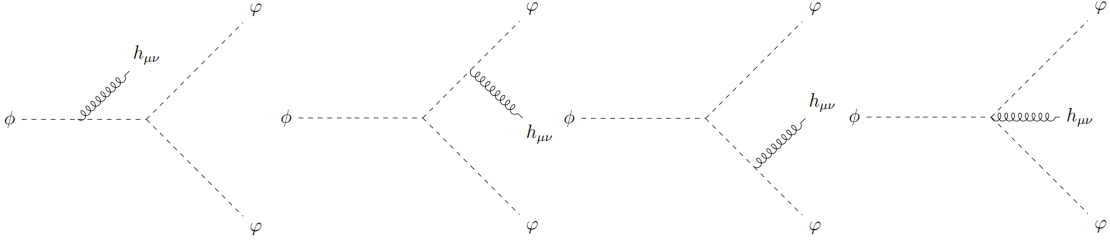


Figure 2. Inflaton decays into a pair of φ and a graviton $h_{\mu\nu}$.

In the above expression, we have considered only the contribution of the first mode $j = 1$ in μ_{eff} . The graviton energy spans the range

$$0 < E_\omega \leq m_\phi \left(\frac{1}{2} - 2y^2 \right). \quad (2.23)$$

We see that when $E_\omega \rightarrow m_\phi \left(\frac{1}{2} - 2y^2 \right)$, the decay becomes kinematically forbidden,⁶ and therefore $d\Gamma^{1 \rightarrow 3}/dE_\omega \rightarrow 0$. Note that here E_ω corresponds to the graviton energy at emission, which can be at most half of the inflaton mass in the limit $y \rightarrow 0$.

2.3 Graviton emission from inflaton annihilation

Instead of decay, the transfer of energy to the SM bath during reheating could be dominated by inflaton annihilation, see e.g. Refs. [51, 52] for motivated scenarios. The $2 \rightarrow 2$ annihilation cross section of inflatons in a pair of real scalars φ , in the non-relativistic limit is given by

$$\Gamma^{2 \rightarrow 2} \simeq \frac{\sigma_{\text{eff}}^2 \rho_\phi}{8\pi m_\phi^3}, \quad (2.24)$$

where

$$\sigma_{\text{eff}}^2 \simeq \sigma^2 n(n+2)(n-1)^2 \frac{\varpi}{m_\phi} \sum_{j=1}^{\infty} j |\mathcal{P}_j|^2 \left\langle \left(1 - \frac{4y^2}{j^2} \mathcal{P} \right)^{1/2} \right\rangle \quad (2.25)$$

denotes the effective coupling after averaging inflaton oscillations [17]. We have introduced the Fourier decomposition of the oscillating background field square

$$\phi(t)^2 = \phi_0^2(t) \mathcal{P}^{(2)}(t) = \phi_0^2(t) \sum_{j=1}^{\infty} \mathcal{P}_j^{(2)}(t) e^{-ij\varpi t}. \quad (2.26)$$

The corresponding interaction rate density is $\gamma \equiv \Gamma^{2 \rightarrow 2} \rho_\phi$, and therefore Eq. (2.7) admits the analytical solution [47]

$$\rho_R(a) \simeq \frac{n}{2n-5} \rho_\phi(a_{\text{end}}) \left(\frac{a_{\text{end}}}{a} \right)^{\frac{18}{n+2}} \left[1 - \left(\frac{a_{\text{end}}}{a} \right)^{\frac{2(2n-5)}{2+n}} \right] \left(\frac{a_{\text{end}}}{a_{\text{RH}}} \right)^{\frac{6(n-3)}{n+2}}, \quad (2.27)$$

which in turn implies that during reheating

$$\alpha \equiv \frac{9}{2n+4}, \quad (2.28)$$

for $n \geq 5/2$. Interestingly, for $n = 2$ (and, in general, for $n < 5/2$), the radiation energy density dilutes faster than nonrelativistic matter (i.e. the inflaton), which implies that it cannot overcome the inflaton energy density, and, therefore, the universe cannot become radiation dominated. In the case of annihilation, Fig. 1 also shows the evolution of the energy densities (left) and the temperature of the SM (right) as a function of the scale factor, for $T_{\text{RH}} = 10^{13}$ GeV, and $T_{\text{max}} = 4.3 \times 10^{14}$ GeV for $n = 4$ (top), or $T_{\text{max}} = 1.2 \times 10^{14}$ GeV for $n = 6$ (bottom). It is clear that in the annihilation case, the evolution of radiation or

⁶It was shown in Ref. [50] that graviton bremsstrahlung can also be the source of dark matter production.

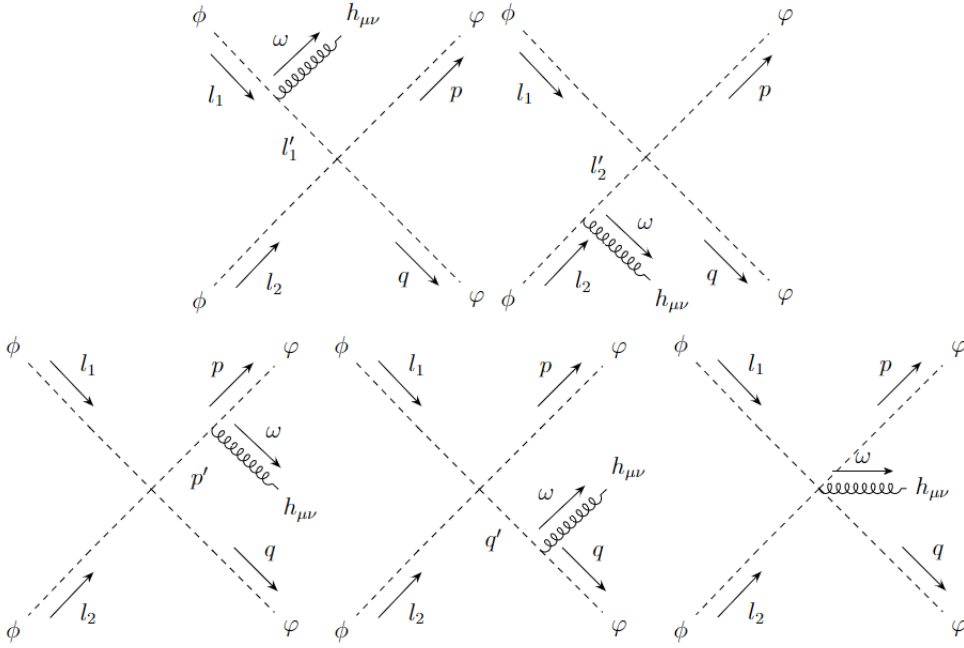


Figure 3. Inflaton annihilation into a pair of φ and a graviton.

temperature is steeper than that in the decay case, which has important implications for the GW spectrum, as will be shown in the next section.

There are some self-consistency conditions that must be met. First, one has to ensure that the inflaton mass satisfies $m_\phi(a) < M_P$ [15], which leads to upper bounds on the reheating energy scale: $m_\phi^{\text{RH}} < M_P (T_{\text{max}}/T_{\text{RH}})^{2(2-n)/3}$ for annihilations and $m_\phi^{\text{RH}} < M_P (T_{\text{max}}/T_{\text{RH}})^{2(2-n)}$ for decays. Alternatively, if one treats m_ϕ^{RH} as a free parameter, the condition $m_\phi(a) < M_P$ also gives upper bounds on the temperature ratio, which reads $(T_{\text{max}}/T_{\text{RH}}) < (m_\phi^{\text{RH}}/M_P)^{3/(4-2n)}$ for annihilations and $(T_{\text{max}}/T_{\text{RH}}) < (m_\phi^{\text{RH}}/M_P)^{1/(4-2n)}$ for decays. Furthermore, we can take advantage of the recent constraint on the inflationary tensor-to-scalar ratio $r < 0.035$, obtained from BICEP/Keck 2018 [53], to derive an upper bound on the inflationary scale, denoted by $H_I < 2.0 \times 10^{-5} M_P$. This upper bound on the inflationary scale, in turn, allows us to establish upper bounds on the reheating temperature. Consequently, for the scenario of annihilation, the upper bounds on the reheating temperature are given by $T_{\text{RH}} < 3.3 \times 10^{15} \text{ GeV} (T_{\text{max}}/T_{\text{RH}})^{-4/3}$ with $n = 4$ and $T_{\text{RH}} < 3.1 \times 10^{15} \text{ GeV} (T_{\text{max}}/T_{\text{RH}})^{-2}$ with $n = 6$. On the other hand, for the inflaton decay scenario, the bounds on the reheating temperature are expressed as $T_{\text{RH}} < 2.8 \times 10^{15} \text{ GeV} (T_{\text{max}}/T_{\text{RH}})^{-4}$ for $n = 4$ and $T_{\text{RH}} < 2.5 \times 10^{15} \text{ GeV} (T_{\text{max}}/T_{\text{RH}})^{-6}$ for $n = 6$. We have checked that the values of T_{max} and T_{RH} shown in Fig. 1 satisfy these constraints.

Similarly to the case of decay, there is a $2 \rightarrow 3$ inflaton annihilation process containing the emission of a graviton, as shown in Fig. 3. Using the Feynman rules and the formalism

as presented in Ref. [14], we obtain the following amplitudes

$$i\mathcal{M}_j^1 = -\frac{i\sigma\phi_0^2}{M_P} \frac{l_{1\mu} l_{1\nu} \epsilon^{*\mu\nu}}{l_1 \cdot \omega} \mathcal{P}_j^{(2)}, \quad (2.29)$$

$$i\mathcal{M}_j^2 = -\frac{i\sigma\phi_0^2}{M_P} \frac{l_{2\mu} l_{2\nu} \epsilon^{*\mu\nu}}{l_2 \cdot \omega} \mathcal{P}_j^{(2)}, \quad (2.30)$$

$$i\mathcal{M}_j^3 = \frac{i\sigma\phi_0^2}{M_P} \frac{p_\mu p_\nu \epsilon^{*\mu\nu}}{p \cdot \omega} \mathcal{P}_j^{(2)}, \quad (2.31)$$

$$i\mathcal{M}_j^4 = \frac{i\sigma\phi_0^2}{M_P} \frac{q_\mu q_\nu \epsilon^{*\mu\nu}}{q \cdot \omega} \mathcal{P}_j^{(2)}, \quad (2.32)$$

$$i\mathcal{M}_5 \propto \eta_{\mu\nu} \epsilon^{*\mu\nu}, \quad (2.33)$$

where

$$p \cdot \omega = 2m_\phi (E_\omega + E_p - m_\phi), \quad (2.34)$$

$$q \cdot \omega = (l_1 + l_2 - \omega - p) \cdot \omega = 2m_\phi E_\omega - p \cdot \omega, \quad (2.35)$$

and $\epsilon^{\mu\nu}$ are the polarisation tensors of the graviton. Note that \mathcal{M}_5 vanishes due to the traceless condition of the massless graviton, while \mathcal{M}_1 and \mathcal{M}_2 vanish since we assume that the inflaton condensate annihilates with a vanishing three-momentum [14].

The $2 \rightarrow 3$ differential interaction rate reads⁷

$$\frac{d\Gamma^{2 \rightarrow 3}}{dE_\omega} = \frac{2m_\phi}{\rho_\phi(1+w_\phi)} \sum_{j=1}^{\infty} \int |\mathcal{M}_j^{2 \rightarrow 3}|^2 \frac{d\text{PS}^{(3)}}{dE_\omega}, \quad (2.36)$$

leading to

$$\frac{d\Gamma^{2 \rightarrow 3}}{dE_\omega} \simeq \frac{\sigma_{\text{eff}}^2}{16\pi^3} \frac{\rho_\phi}{m_\phi^2 M_P^2} \left[\frac{(1-x)(2-2x+y^2)}{x\beta^{-1}} + \frac{y^2(y^2+4x-4)}{2x} \log\left(\frac{1+\beta}{1-\beta}\right) \right], \quad (2.37)$$

where we have considered only the contribution of the first mode in σ_{eff} , with

$$\beta \equiv \sqrt{1 - \frac{y^2}{1-x}}, \quad (2.38)$$

and the graviton energy in the range

$$0 < E_\omega \leq m_\phi(1-y^2). \quad (2.39)$$

As expected, in the limit $E_\omega \rightarrow m_\phi(1-y^2)$, there is no graviton emission as $2 \rightarrow 3$ annihilations become kinematically forbidden. Note that for annihilation, the graviton energy E_ω can be as large as the inflaton mass in the limit $y \rightarrow 0$, which is twice larger than that from the decay (cf. Eq. (2.23)). We will see in the next section that such distinctions have important implications for the range of frequency for the emitted GWs in the two processes.

⁷Note that there we have $2m_\phi$ since the initial energy for annihilation is twice larger compared to that from the decay, which is defined in Eq. (2.20).

3 Gravitational Wave Spectrum

3.1 Overview

Before analyzing in more detail the spectrum and constraints of GWs generated by bremsstrahlung of gravitons, in this section we summarize the procedure in the case of inflaton decay and scattering, in the simplest case of a quadratic potential $V(\phi) = \frac{1}{2}m_\phi^2 \phi^2$. We refer the reader to Appendix A for the complete treatment, which takes into account the sum over all modes in the case of generic potentials. Although we know that complete reheating is not possible in this scenario for pure scattering [17, 18], this example will help us better understand the context and expected results. Moreover, it is always possible to imagine mixed scenarios, where graviton emission by scattering is independent of the process responsible for reheating, such as gravitational reheating.

The differential Boltzmann equation for the energy density ρ_{GW} stored in the form of graviton radiation generated by inflaton decay is

$$\frac{d}{dt} \left(\frac{d\rho_{\text{GW}}}{dE_\omega} \right) + 4H \frac{d\rho_{\text{GW}}}{dE_\omega} = \frac{\rho_\phi}{m_\phi} \frac{d\Gamma^{1 \rightarrow 3}}{dE_\omega} \times E_\omega, \quad (3.1)$$

where $d\Gamma^{1 \rightarrow 3}/dE_\omega$ is given by Eq. (2.21). This equation can be rewritten as

$$\frac{d}{da} \left(a^4 \frac{d\rho_{\text{GW}}}{dE_\omega} \right) = \frac{a^3}{H} \frac{\rho_\phi}{m_\phi} \frac{d\Gamma^{1 \rightarrow 3}}{dE_\omega} \times E_\omega, \quad (3.2)$$

which, in the limit $m, E_\omega \ll m_\phi$, admits the approximate analytical solution

$$\left. \frac{d\rho_{\text{GW}}}{dE_\omega} \right|_{a_{\text{RH}}} \simeq \frac{\sqrt{3}}{160\pi^3} \frac{\mu^2 \sqrt{\rho_{\text{RH}}}}{M_P}, \quad (3.3)$$

where we used $\rho_\phi(a) = \rho_{\text{RH}} \left(\frac{a_{\text{RH}}}{a} \right)^3$ in the case of a quadratic potential. To obtain the gravitational energy density today Ω_{GW}^0 , at energy E_ω , we need to apply the redshift $(a_{\text{RH}}/a_0)^4$ for the energy density and a_{RH}/a_0 for the graviton energy. We then have

$$\Omega_{\text{GW}}^0 = \frac{1}{\rho_c^0} \left. \frac{d\rho_{\text{GW}}}{d \ln E_\omega} \right|_{a_0} = \frac{\sqrt{3}}{160\pi^3} \frac{\mu^2 \rho_R^0}{M_P \rho_c^0 \sqrt{\rho_{\text{RH}}}} \times E_\omega, \quad (3.4)$$

where $\Omega_R^0 = \frac{\rho_R^0}{\rho_c^0}$ is the relative radiation density today, $\rho_c^0 \simeq 1.05 \times 10^{-5} h^2 \text{ GeV/cm}^3$ the critical density at present, and we have used $a_{\text{RH}}/a_0 = (\rho_R^0/\rho_{\text{RH}})^{1/4}$. Alternatively, expressing Eq. (3.4) as function of the frequency defined by $E_\omega(a) = 2\pi f \frac{a_0}{a}$, we obtain

$$\Omega_{\text{GW}}^{1 \rightarrow 3} h^2 \simeq 10^{-20} \left(\frac{10^{10} \text{ GeV}}{T_{\text{RH}}} \right) \left(\frac{\mu}{10^{10} \text{ GeV}} \right)^2 \left(\frac{f}{10^8 \text{ Hz}} \right), \quad (3.5)$$

with $h \simeq 0.67$ the present dimensionless Hubble parameter. Now, if one considers that the reheating is *also* given by the same decaying channel, we can express the GW spectrum completely as a function of T_{RH} (or μ) considering $\Gamma^{1 \rightarrow 2} = \frac{\mu^2}{8\pi m_\phi}$ from Eq. (2.13), and $\rho_{\text{RH}} \simeq \Gamma_\phi^2 M_P^2$. In this case, $\mu = 10^{10} \text{ GeV}$ gives $T_{\text{RH}} \sim 10^{12} \text{ GeV}$ with $m_\phi \simeq 10^{13} \text{ GeV}$. We note that Eq. (3.5) agrees with the earlier result presented in Ref. [14].

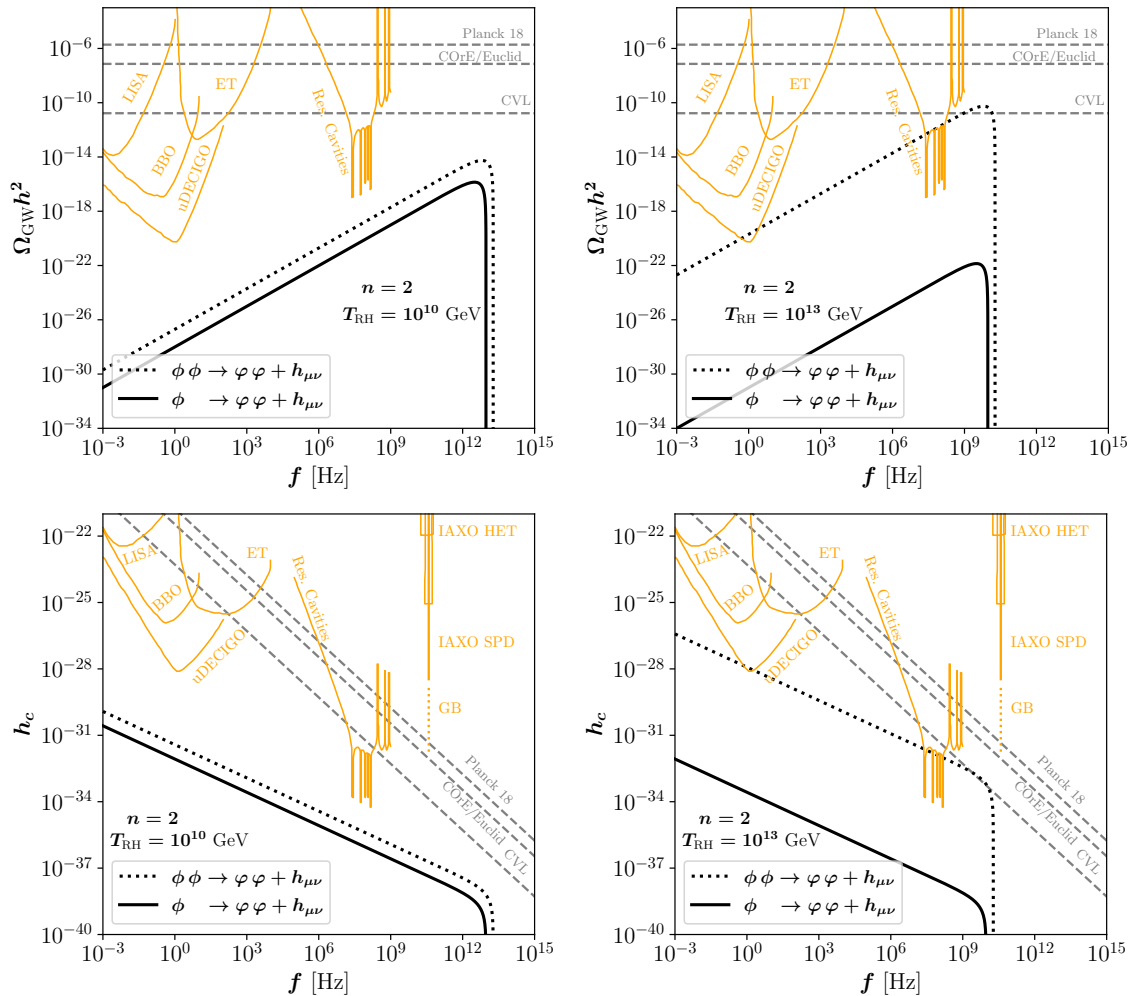


Figure 4. GW spectrum (top) and GW strain (bottom) for the quadratic inflaton potential $n = 2$ with $T_{\text{RH}} = 10^{10}$ GeV (left) and $T_{\text{RH}} = 10^{13}$ GeV (right). Solid black lines represent the signal for inflaton decays with $\mu = 10^{10}$ GeV whereas dashed black lines represent the signal for inflaton scattering with $\sigma = 1$. Sensitivities of future GW detectors are represented by solid orange lines.

For scatterings, the procedure is exactly the same, except that $\Gamma^{1 \rightarrow 3}$ must be replaced by $\Gamma^{2 \rightarrow 3}$ and $m_\phi \rightarrow 2m_\phi$ for annihilation in Eq. (3.1). We then obtain

$$\Omega_{\text{GW}}^{2 \rightarrow 3} h^2 \simeq 10^{-19} \sigma^2 \left(\frac{T_{\text{RH}}}{10^{10} \text{ GeV}} \right)^{\frac{7}{3}} \left(\frac{\rho_{\text{end}}}{6.25 \times 10^{62} \text{ GeV}^4} \right)^{\frac{1}{6}} \left(\frac{10^{13} \text{ GeV}}{m_\phi} \right)^2 \left(\frac{f}{10^8 \text{ Hz}} \right), \quad (3.6)$$

where ρ_{end} represents the energy density stored in the inflaton field at the end of inflation. We normalized Eq. (3.6) with parameters typical of the T -model α -attractors, that is, $\rho_{\text{end}} \sim (5 \times 10^{15})^4 \text{ GeV}^4$ and $m_\phi \sim 10^{13} \text{ GeV}$. For the sake of completeness, we report in Appendix A the complete expression summed over all the inflaton oscillatory modes for a generic potential $V(\phi) \propto \phi^n$.

We illustrate in the top left panel of Fig. 4 the GW spectrum predicted for inflaton

decay (solid black line) and scattering (dotted black line) assuming $\mu = 10^{10}$ GeV, $\sigma = 1$, $T_{\text{RH}} = 10^{10}$ GeV and $n = 2$. We note that the spectra (in the low-frequency regime) nicely match the approximate expressions in Eqs. (3.5) and (3.6), respectively. As mentioned in the previous section, the emitted graviton energy from inflaton annihilation can be twice as large as that from the decay, and consequently, the upper limit of the GW frequency can be twice as large. This explains why the dotted curve (annihilation) peaks at a frequency twice as large as the solid line (decay).

In addition, we overlay several proposed high-frequency GW detectors⁸ with high sensitivity in the figure. These include LISA [55], the Einstein Telescope (ET) [56–59], the Big Bang Observer (BBO) [60–62], ultimate DECIGO (uDECIGO) [63, 64], GW-electromagnetic wave conversion in vacuum (solid) and in a Gaussian beam (GB) (dotted) [7, 65], resonant cavities [66–68], and the International Axion Observatory (IAXO) [69, 70]. Sensitivity curves for these detectors were adapted from Refs. [7, 9]. The energy stored in GWs exhibits characteristics similar to those of dark radiation, which, in turn, contributes to the effective number of neutrino species, denoted N_{eff} .⁹ In this paper, we present a compilation of various constraints related to this phenomenon. The Planck 2018 mission provides valuable information, establishing a 95% CL result of $N_{\text{eff}} = 2.99 \pm 0.34$ [49]. Future experiments, such as CORe [72] and Euclid [73], are expected to significantly enhance these constraints at the 2σ level, resulting in $\Delta N_{\text{eff}} \lesssim 0.013$. It is also interesting to mention a bound of $\Delta N_{\text{eff}} \lesssim 3 \times 10^{-6}$ reported in Ref. [74] based on a hypothetical cosmic-variance-limited (CVL) CMB polarization experiment. We note that for a reheating temperature as low as 10^{10} GeV, it is not possible to detect graviton bremsstrahlung, even in future experiments.

However, the top right panel of Fig. 4 shows an equivalent result, except for $T_{\text{RH}} = 10^{13}$ GeV, which corresponds roughly to an instantaneous reheating. We then clearly see that the spectrum derived from the scattering, in the case $n = 2$, is larger by orders of magnitude than that generated by the inflaton decay. It is also interesting to note that there is a weak dependence of our results on the parameter n . We have made this explicit in Eq. (A.13) in the case of scattering. Furthermore, in our analysis above, we distinguish between the reheating process, which involves T_{RH} , and the bremsstrahlung process. We can also ask whether it is possible to test what the reheating process is (decay or scattering) by measuring the graviton bremsstrahlung generated during the reheating period. But for that, one needs to look for $n \geq 4$, as reheating is not possible by scattering for $n = 2$, which is the purpose of the following section.

For the sake of completeness, and in order to project sensitivity curves from different GW experiments, it is also convenient to define the dimensionless strain h_c in terms of the

⁸See Ref. [54] for a recent review.

⁹Note that the constraint from N_{eff} on the amplitude of GWs, namely $\Omega_{\text{GW}} h^2 \lesssim 5.6 \times 10^{-6} \Delta N_{\text{eff}}$ only applies for the integrated energy density over logarithmic frequency. However, this is a good approximation over a broad range of frequencies and for the GW wavelength well inside the horizon at the moment when the constraint on ΔN_{eff} is established [71].

GW spectral energy density as [75]

$$h_c(f) \equiv \frac{H_0}{f} \sqrt{\frac{3}{2\pi^2} \Omega_{\text{GW}}(f)} \simeq 1.26 \times 10^{-18} \left(\frac{\text{Hz}}{f} \right) \sqrt{h^2 \Omega_{\text{GW}}(f)}, \quad (3.7)$$

where $H_0 \equiv H(T_0) \simeq 1.44 \times 10^{-42}$ GeV is the present-day Hubble parameter [49]. As an illustration, in Fig. 4 (bottom) we depict the strain parameter h_c as a function of frequency f for the same set of parameters as the one used in Fig. 4 (top).

3.2 Combining graviton bremsstrahlung and reheating

In the previous section, the system of Boltzmann equations for the background was solved in the general case, without directly linking the reheating channel with the graviton emission channel. However, to compute the GW spectrum one has to keep track of the evolution of the differential GW energy density ρ_{GW} and radiation ρ_R , and therefore instead of Eqs. (2.6) and (2.7) one has to solve [15]

$$\frac{d\rho_\phi}{dt} + \frac{6n}{2+n} H \rho_\phi = -\frac{2n}{2+n} (\gamma^{(0)} + \gamma^{(1)}), \quad (3.8)$$

$$\frac{d\rho_R}{dt} + 4H \rho_R = +\frac{2n}{2+n} \gamma^{(0)} + \frac{2n}{2+n} \int \frac{d\gamma^{(1)}}{dE_\omega} \frac{E_\phi - E_\omega}{E_\phi} dE_\omega, \quad (3.9)$$

$$\frac{d\rho_{\text{GW}}}{dt} + 4H \rho_{\text{GW}} = +\frac{2n}{2+n} \int \frac{d\gamma^{(1)}}{dE_\omega} \frac{E_\omega}{E_\phi} dE_\omega, \quad (3.10)$$

where E_ω corresponds to the graviton energy at the moment of production, and E_ϕ corresponds to the initial total inflaton energy, either $E_\phi = m_\phi$ for decays or $E_\phi = 2m_\phi$ for annihilations. The term $(E_\phi - E_\omega)/E_\phi$ describes the energy fraction that goes to radiation. The density rates $\gamma^{(0)}$ and $\gamma^{(1)}$ correspond to the cases without and with graviton emission, respectively. More specifically, for inflaton decays, we have $\gamma^{(0)} = \Gamma^{1 \rightarrow 2} \rho_\phi$ and $\gamma^{(1)} = \Gamma^{1 \rightarrow 3} \rho_\phi$, and $\gamma^{(0)} = \Gamma^{2 \rightarrow 2} \rho_\phi$ and $\gamma^{(1)} = \Gamma^{2 \rightarrow 3} \rho_\phi$ for inflaton annihilations.¹⁰

For the GW spectrum, what we need is the differential GW energy density; therefore, it is convenient to write Eq. (3.10) as

$$\frac{d}{da} \frac{d(\rho_{\text{GW}}/\rho_R)}{dE_\omega} \simeq \frac{2n}{2+n} \frac{1}{a H(T_{\text{RH}})} \left(\frac{a_{\text{RH}}}{a} \right)^{\frac{3n}{2+n} - 4\alpha} \left[\frac{d\Gamma^{(1)}}{dE_\omega} \frac{E_\omega}{m_\phi} - \frac{d(\rho_{\text{GW}}/\rho_R)}{dE_\omega} \Gamma^{(0)} \right]. \quad (3.11)$$

Note that E_ω corresponds to the energy at the moment when gravitons are emitted. However, to compute the GW spectrum, we need to consider the redshift and sum over different (redshifted) energies. Therefore, in Eq. (3.11) the change of variable $E_\omega(E'_\omega, a) = E'_\omega \frac{a_{\text{RH}}}{a}$, with E'_ω being the energy at $a = a_{\text{RH}}$, is required, leading to [15]

$$\frac{d}{da} \frac{d(\rho_{\text{GW}}/\rho_R)}{dE'_\omega} \simeq \frac{a_{\text{RH}}}{a} \frac{2n}{2+n} \frac{1}{a H(T_{\text{RH}})} \left(\frac{a_{\text{RH}}}{a} \right)^{\frac{3n}{2+n} - 4\alpha} \left[\frac{d\Gamma^{(1)}}{dE'_\omega} \frac{E'_\omega}{m_\phi} - \frac{a}{a_{\text{RH}}} \frac{d(\rho_{\text{GW}}/\rho_R)}{dE'_\omega} \Gamma^{(0)} \right], \quad (3.12)$$

¹⁰Note that if the decay final states have N degrees of freedom, one shall multiply a factor N in the rates.

where the extra overall factor a_{RH}/a arises from the Jacobian related to the changing of variables.

The solution for Eq. (3.12) in the case of inflaton decays was recently reported in Ref. [15]. In this work, we focus on the yet unexplored case of inflaton annihilation. In that case, Eq. (3.12) admits analytical solutions for different values of n . Recalling that reheating by inflaton annihilation is not viable in the case $n = 2$, we explore the scenarios with $n = 4$ and $n = 6$.

- For $n = 4$, it follows that

$$\frac{d(\rho_{\text{GW}}/\rho_R)}{dE'_\omega} \simeq \frac{2 m_\phi^{\text{RH}}}{M_P^2 \pi^2} \left(1 - \frac{E'_\omega}{m_\phi^{\text{RH}}}\right)^2 \left[\left(\frac{T_{\text{max}}}{T_{\text{RH}}}\right)^{8/9} - 1 \right], \quad (3.13)$$

for $0 \leq E'_\omega \leq m_\phi^{\text{RH}}$.

- For $n = 6$, one has

$$\begin{aligned} \frac{d(\rho_{\text{GW}}/\rho_R)}{dE'_\omega} \simeq \frac{3 m_\phi^{\text{RH}}}{2\pi^2 M_P^2} & \left[\left(\frac{T_{\text{max}}}{T_{\text{RH}}}\right)^{16/9} - 1 \right] - 4 \frac{E'_\omega}{m_\phi^{\text{RH}}} \left[\left(\frac{T_{\text{max}}}{T_{\text{RH}}}\right)^{8/9} - 1 \right] \\ & + \frac{16}{9} \left(\frac{E'_\omega}{m_\phi^{\text{RH}}}\right)^2 \log \left(\frac{T_{\text{max}}}{T_{\text{RH}}}\right) \end{aligned} \quad (3.14)$$

for $0 \leq E'_\omega \leq m_\phi^{\text{RH}}$, while for $m_\phi^{\text{RH}} \leq E'_\omega \leq m_\phi^{\text{RH}} \left(\frac{T_{\text{max}}}{T_{\text{RH}}}\right)^{8/9}$ it becomes

$$\begin{aligned} \frac{d(\rho_{\text{GW}}/\rho_R)}{dE'_\omega} \simeq \frac{3 m_\phi^{\text{RH}}}{2\pi^2 M_P^2} & \left[\left(\frac{T_{\text{max}}}{T_{\text{RH}}}\right)^{16/9} - 4 \frac{E'_\omega}{m_\phi^{\text{RH}}} \left(\frac{T_{\text{max}}}{T_{\text{RH}}}\right)^{8/9} \right. \\ & \left. + \left(\frac{E'_\omega}{m_\phi^{\text{RH}}}\right)^2 \left(3 + 2 \log \left[\frac{m_\phi^{\text{RH}}}{E'_\omega} \left(\frac{T_{\text{max}}}{T_{\text{RH}}}\right)^{8/9} \right] \right) \right]. \end{aligned} \quad (3.15)$$

Several comments on the regimes for E'_ω shown above are in order. Note that the graviton energy at emission always lies in the range $0 < E_\omega \leq m_\phi(a)$, which together with $E'_\omega = E_\omega a/a_{\text{RH}}$ implies $0 < E'_\omega \leq m_\phi^{\text{RH}} (a/a_{\text{RH}})^{2(n-4)/(n+2)}$. Subsequently, for $n = 4$, one has $0 < E'_\omega \leq m_\phi^{\text{RH}}$. However, for $n = 6$, there are two energy regimes: low-energy gravitons in the range $0 < E'_\omega \leq m_\phi^{\text{RH}}$ can be produced during the entire reheating period, while high-energy gravitons with $m_\phi^{\text{RH}} \leq E'_\omega \leq m_\phi^{\text{RH}} (T_{\text{max}}/T_{\text{RH}})^{8/9}$ can only be produced in the last stages of reheating. Additionally, we notice that the GW spectrum features a smaller boost proportional to powers of the ratio $T_{\text{max}}/T_{\text{RH}}$, compared to the decay case, as for annihilations the entropy dilution is more prominent, as shown in Fig. 1.

The primordial GW spectrum $\Omega_{\text{GW}}(f)$ at present per logarithmic frequency f is

$$\Omega_{\text{GW}}(f) = \Omega_\gamma^{(0)} \frac{g_\star(T_{\text{RH}})}{g_\star(T_0)} \left[\frac{g_{\star s}(T_0)}{g_{\star s}(T_{\text{RH}})} \right]^{4/3} \frac{d(\rho_{\text{GW}}(T_{\text{RH}})/\rho_R(T_{\text{RH}}))}{d \ln E'_\omega}, \quad (3.16)$$

where $\Omega_\gamma^{(0)} h^2 \simeq 2.47 \times 10^{-5}$ is the current photon density, $T_0 \simeq 2.73$ K is the CMB temperature [49], and $g_{\star s}(T)$ is the number of relativistic degrees of freedom that contribute

to the SM entropy. The present GW frequency is associated with the graviton energy E'_ω at the end of reheating via

$$f = \frac{E'_\omega}{2\pi} \frac{a_{\text{RH}}}{a_0} = \frac{E'_\omega}{2\pi} \frac{T_0}{T_{\text{RH}}} \left[\frac{g_{\star s}(T_0)}{g_{\star s}(T_{\text{RH}})} \right]^{1/3}, \quad (3.17)$$

considering the redshift of the graviton energy from the end of reheating and the present epoch. Note that the frequency is bounded from above since the graviton at production could carry at most half of the total inflaton energy, namely $E_\omega(a) \leq m_\phi(a)$ for inflaton annihilation, which translates into

$$f \leq \frac{m_\phi^{\text{RH}}}{2\pi} \frac{a_{\text{RH}}}{a_0} \left(\frac{a_{\text{RH}}}{a} \right)^{\frac{2(n-4)}{n+2}} \leq \frac{m_\phi^{\text{RH}}}{2\pi} \frac{T_0}{T_{\text{RH}}} \left[\frac{g_{\star s}(T_0)}{g_{\star s}(T_{\text{RH}})} \right]^{1/3} \times \begin{cases} 1 & \text{for } n \leq 4, \\ \left(\frac{T_{\text{max}}}{T_{\text{RH}}} \right)^{\frac{2(n-4)}{\alpha(n+2)}} & \text{for } n > 4. \end{cases} \quad (3.18)$$

In the case of an inflaton decay, $E_\omega(a) \leq m_\phi(a)/2$, leading to an additional $1/2$ on the right-hand side of Eq. (3.18).

In Fig. 5, we present the GW spectrum for the benchmark parameters: ① $T_{\text{RH}} = 10^{13}$ GeV, $m_\phi^{\text{RH}} = 1.1 \times 10^{11}$ GeV, $T_{\text{max}}/T_{\text{RH}} = 43$ (for $n = 4$) and $T_{\text{RH}} = 10^{13}$ GeV, $m_\phi^{\text{RH}} = 2.6 \times 10^{10}$ GeV, $T_{\text{max}}/T_{\text{RH}} = 12$ (for $n = 6$), and ② $m_\phi^{\text{RH}} = 5 \times 10^{16}$ GeV, $T_{\text{RH}} = 5 \times 10^{13}$ GeV and $T_{\text{max}}/T_{\text{RH}} = 4$ for both $n = 4$ and $n = 6$. Note that the parameters in ① are derived from the α -attractor T -model (cf. Fig. 1). In addition, the model parameters we have considered satisfy the limits detailed in Section 2.3. GW signals are depicted for two different cases: $n = 6$ (solid black line) and $n = 4$ (dotted black line). For the case with $n = 6$, the signal shows a boost factor $\propto (T_{\text{max}}/T_{\text{RH}})^{16/9}$ (cf. Eq. (3.14)), which exceeds the boost factor $\propto (T_{\text{max}}/T_{\text{RH}})^{8/9}$ observed in the case $n = 4$ (cf. Eq. (3.13)), and therefore the strain of the GW spectrum corresponding to $n = 6$ is expected to be higher. (Note that this conclusion is based on the same model parameters, that is, ②.) Furthermore, it should be noted that the upper limit of the GW frequency is higher for $n = 6$ compared to the case with $n = 4$, as explained by Eq. (3.18). The wider range of frequencies for $n = 6$ adds to the distinction between the two cases in the spectrum. These results suggest that the parameter space of the inflaton annihilation reheating scenario might be probed by next-generation GW detectors as gravitational cavities and ΔN_{eff} experiments.

To facilitate comparison of our results on inflaton annihilation with inflaton decays, in Fig. 6, we show the GW spectrum of several benchmark parameters. In the left panel with $n = 4$, the parameters considered are: ① $T_{\text{RH}} = 10^{13}$ GeV, $m_\phi^{\text{RH}} = 1.1 \times 10^{11}$ GeV, $T_{\text{max}}/T_{\text{RH}} = 3.6$ (for decay) and $T_{\text{RH}} = 10^{13}$ GeV, $m_\phi^{\text{RH}} = 1.1 \times 10^{11}$ GeV, $T_{\text{max}}/T_{\text{RH}} = 43$ (for annihilation); ② $T_{\text{RH}} = 10^{12}$ GeV, $T_{\text{max}}/T_{\text{RH}} = 7$, $m_\phi^{\text{RH}} = 8 \times 10^{14}$ GeV for both decay and annihilation. In the right frame with $n = 6$: ① $T_{\text{RH}} = 10^{13}$ GeV, $m_\phi^{\text{RH}} = 2.6 \times 10^{10}$ GeV, $T_{\text{max}}/T_{\text{RH}} = 2.4$ (for decay) and $T_{\text{RH}} = 10^{13}$ GeV, $m_\phi^{\text{RH}} = 2.6 \times 10^{10}$ GeV, $T_{\text{max}}/T_{\text{RH}} = 12$ (for annihilation); ② $T_{\text{RH}} = 3 \times 10^{12}$ GeV, $T_{\text{max}}/T_{\text{RH}} = 3$, $m_\phi^{\text{RH}} = 3 \times 10^{14}$ GeV for both decay and annihilation.

Solid lines correspond to the case where the inflaton annihilates, while dotted curves correspond to the case of decay. For $n = 4$, we notice that the GW frequency in the

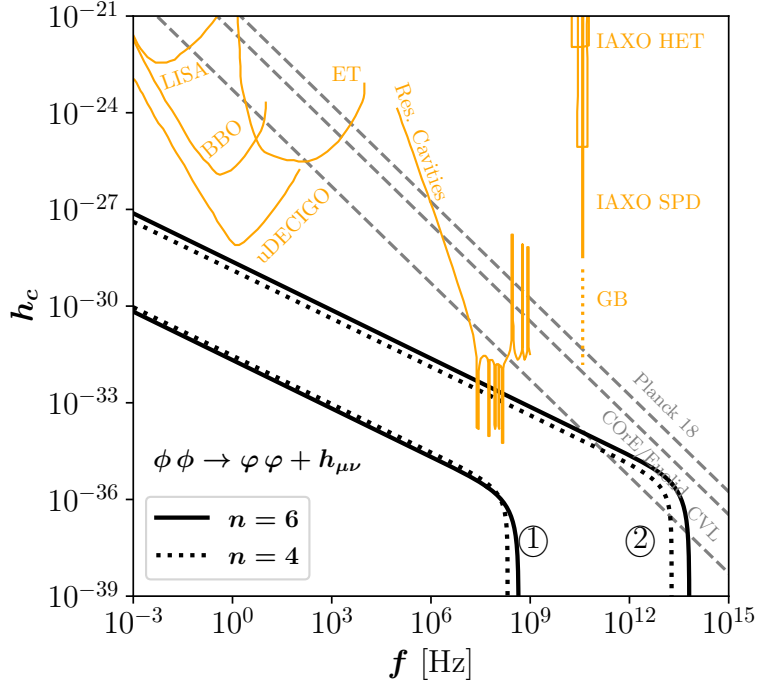


Figure 5. GW signature from graviton bremsstrahlung via inflaton annihilation during reheating, assuming the following parameters: ① $T_{\text{RH}} = 10^{13}$ GeV, $m_{\phi}^{\text{RH}} = 1.1 \times 10^{11}$ GeV, $T_{\text{max}}/T_{\text{RH}} = 43$ (for $n = 4$) and $T_{\text{RH}} = 10^{13}$ GeV, $m_{\phi}^{\text{RH}} = 2.6 \times 10^{10}$ GeV, $T_{\text{max}}/T_{\text{RH}} = 12$ (for $n = 6$); ② $m_{\phi}^{\text{RH}} = 5 \times 10^{16}$ GeV, $T_{\text{RH}} = 5 \times 10^{13}$ GeV and $T_{\text{max}}/T_{\text{RH}} = 4$ for both $n = 4$ and $n = 6$.

annihilation scenario can be shifted to a higher value compared to the decay model; this is because the maximum energy of the emitted graviton can be twice higher in the annihilation scenario. In the context of the same model parameters, e.g., ②, we find that the GW amplitude in the case of annihilation is smaller than that in the case of decay. This is because for annihilation, the spectrum has an enhancement during reheating $\propto (T_{\text{max}}/T_{\text{RH}})^{8/9}$ (cf. Eq. (3.13)) that is lower than that in the case of decays, where the enhancement is $\propto (T_{\text{max}}/T_{\text{RH}})^{8/3}$ [15]. This distinctive enhancement originates from the evolution of the temperature and hence the dilution effect during reheating. Due to the steeper slope of temperature evolution in the annihilation scenario (cf. Fig. 1), it is expected that for larger n , the dilution effect becomes more prominent. Consequently, the spectrum in the annihilation model becomes suppressed compared to that in the decay case, as shown in the figure. With a progressive increase in the parameter n , the distinction between the GW spectra in the two scenarios considered becomes increasingly pronounced, as illustrated in the right panel. For the aforementioned benchmark parameters, we notice that the GW signature might be within the sensitivity of future cavity experiments. Specifically, for $n = 6$, we observe that the GW spectrum exhibits a discernible signal that may be detectable by resonant cavity detectors. On the contrary, the amplitude of the GW spectrum in the annihilation scenario is considerably lower and lies beyond the range of sensitivity of the cavity detectors.

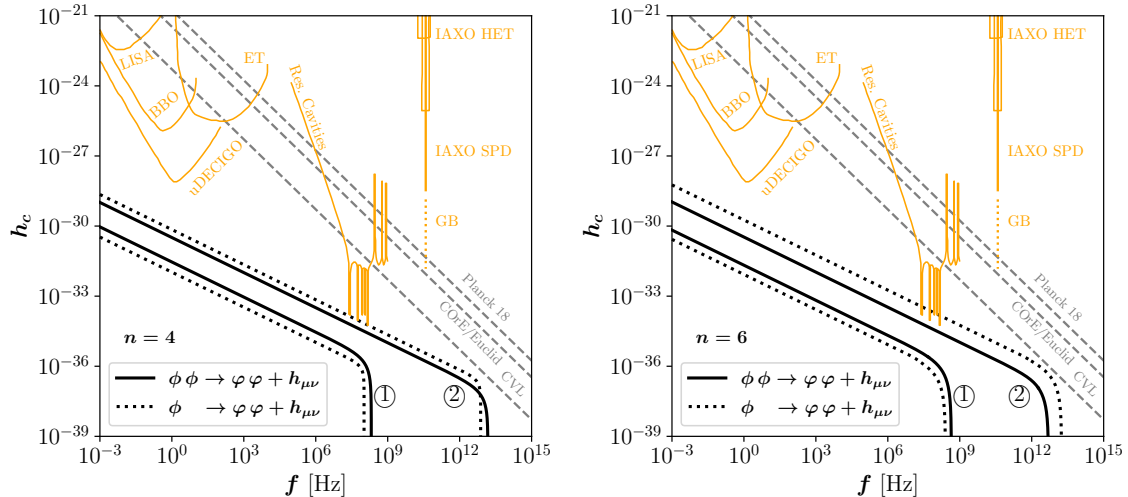


Figure 6. Comparison for GW signature from graviton bremsstrahlung via inflaton decay and annihilation during reheating. The left and right frames correspond to the spectrum with $n = 4$ and $n = 6$, respectively.

In the event that a null signal is observed in future high-frequency GW measurements, it would enable the exclusion of certain regions of the parameter space. Consequently, our proposed approach, utilizing bremsstrahlung-induced GWs, could give useful information on the reheating dynamics.

4 Conclusions

In this study, we have revisited graviton bremsstrahlung during the phase of inflationary reheating in the presence of an inflaton field ϕ oscillating around a generic monomial potential ϕ^n . Unlike previous analyses, we have examined for the first time the gravitational wave (GW) spectrum within the context of a reheating scenario involving inflaton annihilations. We calculated the corresponding graviton emission rate, which is presented in Eq. (2.37) and the corresponding GW spectra are illustrated in Fig. 4. This is complementary to previous studies where only inflaton decays were assumed [11–16].

We showed first that, depending on the reheating temperature, in the case of a quadratic potential with $n = 2$, the scattering of the inflaton can give a much larger amount of graviton through bremsstrahlung than the decay channel, as one can see in the right panel of Fig. 4. Interestingly, these spectra could be in the region probed by next-generation GW observatories.

We then concentrated our study on the assumption that the channel responsible for the bremsstrahlung is also responsible for the reheating process. The reheating temperature is then directly related to the GW spectrum. For $n > 2$ we found that the GW spectrum features a power-law enhancement on the ratio T_{\max}/T_{RH} , whose effect becomes more prominent with increasing n , as shown in Fig. 5. Compared to the inflaton decay scenario, we found that the GW spectrum exhibits distinct characteristics, depicted in

Fig. 6, which could potentially allow us to distinguish between decays and annihilations. These distinctions arise from the disparate scaling behaviors exhibited by the radiation released during the reheating process (cf. Fig. 1), which behaves as a dilution effect for the GW spectrum. Particularly noteworthy is the fact that, for certain model parameters, the GW spectrum in the annihilation scenario is smaller than in the decay case, where the latter could fall within the detectability range of future cavity detectors. Our results thus suggest a new potential avenue for probing the parameter space of reheating by utilizing bremsstrahlung-induced GWs.

Acknowledgments

The authors want to thank Basabendu Barman, Mathias Pierre and Óscar Zapata for very fruitful discussions. N.B. received funding from the Spanish FEDER / MCIU-AEI under the grant FPA2017-84543-P and thanks the ICTP staff for their hospitality during his stay when this study was completed. S.C. and Y.M. acknowledge the support of the Institut Pascal at Université Paris-Saclay during the Paris-Saclay Astroparticle Symposium 2023, with the support of the P2IO Laboratory of Excellence (program “Investissements d’avenir” ANR-11-IDEX-0003-01 Paris-Saclay and ANR-10-LABX-0038), the P2I axis of the Graduate School of Physics of Université Paris-Saclay, as well as IJCLab, CEA, IAS, OSUPS, and the IN2P3 master project UCMN. Y.X. has received support from the Cluster of Excellence “Precision Physics, Fundamental Interactions, and Structure of Matter” (PRISMA⁺ EXC 2118/1) funded by the Deutsche Forschungsgemeinschaft (DFG, German Research Foundation) within the German Excellence Strategy (Project No. 390831469). This project has received funding and support from the European Union’s Horizon 2020 research and innovation program under the Marie Skłodowska-Curie grant agreement No. 860881-HIDDeN.

A Graviton Bremsstrahlung for a Monomial Potential

We can solve Eq. (3.2) for a generic potential of the inflaton during reheating $V(\phi) = \lambda M_P^4 \left(\frac{\phi}{M_P}\right)^n$. We obtain the generic solution for the $1 \rightarrow 3$ process

$$\left. \frac{d\rho_{\text{GW}}}{dE_\omega} \right|_{a_{\text{RH}}}^{1 \rightarrow 3} = \frac{\sqrt{3}\mu^2 M_P}{32\pi^3} \alpha_n^2 \left(\frac{\rho_{\text{RH}}}{M_P^4}\right)^{\frac{1}{2}} \int_{a_{\text{end}}}^{a_{\text{RH}}} \frac{da}{a_{\text{RH}}} \left(\frac{a}{a_{\text{RH}}}\right)^{\frac{6}{n+2}} \sum_{j=1}^{\infty} j^2 |\mathcal{P}_j|^2 (1 - 2x_j(a))^2, \quad (\text{A.1})$$

for $y \rightarrow 0$. For the case $n = 2$, the frequency of the oscillation is fixed as $\varpi = m_\phi$, and there is only one mode in the Fourier decomposition corresponding to $j = 1$ associated with the coefficient $\mathcal{P}_1 = \frac{1}{2}$. Hence, ignoring the redshift dependence of x_j ,¹¹ we recover

$$\left. \frac{d\rho_{\text{GW}}}{dE_\omega} \right|_{a_{\text{RH}}}^{1 \rightarrow 3} = \frac{\sqrt{3}\mu^2 M_P}{160\pi^3} \left(\frac{\rho_{\text{RH}}}{M_P^4}\right)^{1/2} \left[1 - \left(\frac{a_{\text{end}}}{a_{\text{RH}}}\right)^{5/2}\right] \left(1 - 2\frac{E_\omega}{m_\phi}\right)^2. \quad (\text{A.2})$$

¹¹For a complete treatment of the energy redshift during reheating we refer the reader to Ref. [15].

The relic density of GWs is obtained by

$$\Omega_{\text{GW}}^0 h^2 = \frac{h^2}{\rho_c^0} \left. \frac{d\rho_{\text{GW}}}{dE_\omega} \right|_{a_{\text{RH}}} \left(\frac{a_{\text{RH}}}{a_0} \right)^4 \times E_\omega(a_{\text{RH}}), \quad (\text{A.3})$$

where we can relate the present energy of the gravitons with the current frequency of the GW, $E_\omega(a_{\text{RH}}) = 2\pi f(a_0/a_{\text{RH}})$. This leads in case $n = 2$ to the following relic density for $a_{\text{end}} \ll a_{\text{RH}}$ and $E_\omega(a_{\text{RH}}) \ll m_\phi$

$$\Omega_{\text{GW}}^0 h^2 \simeq \frac{h^2 \mu^2 \sqrt{3}}{80\pi^2} \times \frac{f}{M_P} \times \frac{\Omega_R^0}{(\rho_{\text{RH}} \rho_R^0)^{1/4}}. \quad (\text{A.4})$$

For the generic case $n > 2$, the integration of the energy density spectrum is generally more involved, as the energy in each mode is time dependent, leading to mode-dependent boundaries of the integral. We give an approximate solution for a part of the spectrum where $E_\omega(a_{\text{RH}}) \ll \omega(a_{\text{RH}})$. In this case, all the modes contribute similarly to the production of gravitons until the end of reheating, with a contribution proportional to $j^2 |\mathcal{P}_j|^2$ for each mode j

$$\left. \frac{d\rho_{\text{GW}}}{dE_\omega} \right|_{a_{\text{RH}}}^{1 \rightarrow 3} \simeq \frac{\sqrt{3} \mu^2 M_P}{32\pi^3} \alpha_n^2 \left(\frac{\rho_{\text{RH}}}{M_P^4} \right)^{1/2} \left(\frac{n+2}{n+8} \right) \left[1 - \left(\frac{a_{\text{end}}}{a_{\text{RH}}} \right)^{\frac{n+8}{n+2}} \right] \sum_{j=1}^{\infty} j^2 |\mathcal{P}_j|^2 \quad (\text{A.5})$$

Hence, we see that in the low-frequency limit, the influence of the shape of the inflaton potential is only a change in the amplitude of the spectrum

$$\frac{\Omega_{\text{GW}}^{n>2}}{\Omega_{\text{GW}}^{n=2}} \simeq \frac{n+2}{n+8} \frac{\alpha_n^2}{5} \sum_{j=1}^{\infty} j^2 |\mathcal{P}_j|^2. \quad (\text{A.6})$$

Computing the integral with all modes provides a peak structure in the GW spectrum that we did not consider in our analysis.

Now, we consider the scattering channel. We can obtain similar expressions for the $2 \rightarrow 3$ process

$$\left. \frac{d\rho_{\text{GW}}}{dE_\omega} \right|_{a_{\text{RH}}}^{2 \rightarrow 3} = \frac{\sqrt{3} \sigma^2 M_P^3}{8\pi^3 \lambda^{2/n}} \alpha_n^2 \left(\frac{\rho_{\text{RH}}}{M_P^4} \right)^{\frac{n+4}{2n}} \int_{a_{\text{end}}}^{a_{\text{RH}}} \frac{da}{a_{\text{RH}}} \left(\frac{a}{a_{\text{RH}}} \right)^{-\frac{6}{n+2}} \sum_{j=1}^{\infty} j^2 |\mathcal{P}_j^{(2)}|^2 (1 - x_j(a))^2. \quad (\text{A.7})$$

In the case $n = 2$, we recover

$$\left. \frac{d\rho_{\text{GW}}}{dE_\omega} \right|_{a_{\text{RH}}}^{2 \rightarrow 3} = \frac{\sqrt{3} \sigma^2 M_P^3}{16\pi^3 \lambda} \left(\frac{\rho_{\text{RH}}}{M_P^4} \right)^{3/2} \left[\left(\frac{a_{\text{RH}}}{a_{\text{end}}} \right)^{1/2} - 1 \right] \left(1 - \frac{E_\omega}{m_\phi} \right)^2, \quad (\text{A.8})$$

leading, in the limit $a_{\text{end}} \ll a_{\text{RH}}$ and $E_\omega(a_{\text{RH}}) \ll m_\phi$, to

$$\Omega_{\text{GW}}^0 h^2 \simeq \frac{h^2 \sigma^2 \sqrt{3}}{4\pi^2} \times \frac{f}{M_P} \times \frac{\rho_{\text{end}}^{1/6} \rho_{\text{RH}}^{7/12} \Omega_R^0}{m_\phi^2 (\rho_R^0)^{1/4}}, \quad (\text{A.9})$$

where we have used the relation $\lambda = m_\phi^2 / (2M_P^2)$ considering the quadratic potential of the inflaton.

In the general case $n > 2$, again the situation is more complicated as the frequency of the background oscillations evolves with time. However, we give an approximate solution for a part of the spectrum where $E_\omega(a_{\text{RH}}) \ll \omega(a_{\text{RH}})$

$$\frac{d\rho_{\text{GW}}}{dE_\omega} \Big|_{a_{\text{RH}}}^{2 \rightarrow 3} \simeq \frac{\sqrt{3}\sigma^2 M_P^3}{8\pi^3 \lambda^{1/2}} \alpha_4^2 \left(\frac{\rho_{\text{RH}}}{M_P^4} \right) \ln \left(\frac{\rho_{\text{end}}}{\rho_{\text{RH}}} \right) \sum_{j=1}^{\infty} j^2 \left| \mathcal{P}_j^{(2)} \right|^2 \quad (\text{A.10})$$

for $n = 4$, or

$$\frac{d\rho_{\text{GW}}}{dE_\omega} \Big|_{a_{\text{RH}}}^{2 \rightarrow 3} \simeq \frac{n+2}{n-4} \frac{\sqrt{3}\sigma^2 M_P^3}{8\pi^3 \lambda^{2/n}} \alpha_n^2 \left(\frac{\rho_{\text{RH}}}{M_P^4} \right)^{\frac{n+4}{2n}} \left[1 - \left(\frac{a_{\text{end}}}{a_{\text{RH}}} \right)^{\frac{n-4}{n+2}} \right] \sum_{j=1}^{\infty} j^2 \left| \mathcal{P}_j^{(2)} \right|^2 \quad (\text{A.11})$$

for $n > 4$. In the low-frequency limit, the influence of the shape of the inflaton potential for the $2 \rightarrow 3$ process again is only a change in the amplitude of the spectrum

$$\frac{\Omega_{\text{GW}}^{n=4}}{\Omega_{\text{GW}}^{n=2}} \simeq 2\alpha_4^2 \lambda^{\frac{1}{2}} \sum_{j=1}^{\infty} j^2 \left| \mathcal{P}_j^{(2)} \right|^2 \quad (n = 4), \quad (\text{A.12})$$

$$\frac{\Omega_{\text{GW}}^{n>2}}{\Omega_{\text{GW}}^{n=2}} \simeq \frac{n+2}{n-4} \frac{2\alpha_n^2}{\lambda^{\frac{2-n}{n}}} \sum_{j=1}^{\infty} j^2 \left| \mathcal{P}_j^{(2)} \right|^2 \quad (n > 4). \quad (\text{A.13})$$

References

- [1] D.H. Lyth and A.R. Liddle, *The primordial density perturbation: Cosmology, inflation and the origin of structure* (2009).
- [2] L. Kofman, A.D. Linde and A.A. Starobinsky, *Towards the theory of reheating after inflation*, *Phys. Rev. D* **56** (1997) 3258 [[hep-ph/9704452](#)].
- [3] S. Weinberg, *Infrared photons and gravitons*, *Phys. Rev.* **140** (1965) B516.
- [4] B.M. Barker, S.N. Gupta and J. Kaskas, *Graviton bremsstrahlung and infrared divergence*, *Phys. Rev.* **182** (1969) 1391.
- [5] J. Ghiglieri and M. Laine, *Gravitational wave background from Standard Model physics: Qualitative features*, *JCAP* **07** (2015) 022 [[1504.02569](#)].
- [6] J. Ghiglieri, G. Jackson, M. Laine and Y. Zhu, *Gravitational wave background from Standard Model physics: Complete leading order*, *JHEP* **07** (2020) 092 [[2004.11392](#)].
- [7] A. Ringwald, J. Schütte-Engel and C. Tamarit, *Gravitational Waves as a Big Bang Thermometer*, *JCAP* **03** (2021) 054 [[2011.04731](#)].
- [8] P. Klose, M. Laine and S. Procacci, *Gravitational wave background from non-Abelian reheating after axion-like inflation*, *JCAP* **05** (2022) 021 [[2201.02317](#)].
- [9] A. Ringwald and C. Tamarit, *Revealing the cosmic history with gravitational waves*, *Phys. Rev. D* **106** (2022) 063027 [[2203.00621](#)].
- [10] J. Ghiglieri, J. Schütte-Engel and E. Speranza, *Freezing-In Gravitational Waves*, [2211.16513](#).
- [11] K. Nakayama and Y. Tang, *Stochastic Gravitational Waves from Particle Origin*, *Phys. Lett. B* **788** (2019) 341 [[1810.04975](#)].

- [12] D. Huang and L. Yin, *Stochastic Gravitational Waves from Inflaton Decays*, *Phys. Rev. D* **100** (2019) 043538 [[1905.08510](#)].
- [13] A. Ghoshal, R. Samanta and G. White, *Bremsstrahlung high-frequency gravitational wave signatures of high-scale nonthermal leptogenesis*, *Phys. Rev. D* **108** (2023) 035019 [[2211.10433](#)].
- [14] B. Barman, N. Bernal, Y. Xu and Ó. Zapata, *Gravitational wave from graviton Bremsstrahlung during reheating*, *JCAP* **05** (2023) 019 [[2301.11345](#)].
- [15] B. Barman, N. Bernal, Y. Xu and Ó. Zapata, *Bremsstrahlung-induced gravitational waves in monomial potentials during reheating*, *Phys. Rev. D* **108** (2023) 083524 [[2305.16388](#)].
- [16] S. Kanemura and K. Kaneta, *Gravitational Waves from Particle Decays during Reheating*, [2310.12023](#).
- [17] M.A.G. Garcia, K. Kaneta, Y. Mambrini and K.A. Olive, *Inflaton Oscillations and Post-Inflationary Reheating*, *JCAP* **04** (2021) 012 [[2012.10756](#)].
- [18] M.A.G. Garcia, K. Kaneta, Y. Mambrini and K.A. Olive, *Reheating and Post-inflationary Production of Dark Matter*, *Phys. Rev. D* **101** (2020) 123507 [[2004.08404](#)].
- [19] B. Barman and N. Bernal, *Gravitational SIMPs*, *JCAP* **06** (2021) 011 [[2104.10699](#)].
- [20] S.Y. Choi, J.S. Shim and H.S. Song, *Factorization and polarization in linearized gravity*, *Phys. Rev. D* **51** (1995) 2751 [[hep-th/9411092](#)].
- [21] M.S. Turner, *Coherent Scalar Field Oscillations in an Expanding Universe*, *Phys. Rev. D* **28** (1983) 1243.
- [22] N. Bernal and Y. Xu, *WIMPs during reheating*, *JCAP* **12** (2022) 017 [[2209.07546](#)].
- [23] A.A. Starobinsky, *A New Type of Isotropic Cosmological Models Without Singularity*, *Phys. Lett. B* **91** (1980) 99.
- [24] M. Drees and Y. Xu, *Small field polynomial inflation: reheating, radiative stability and lower bound*, *JCAP* **09** (2021) 012 [[2104.03977](#)].
- [25] N. Bernal and Y. Xu, *Polynomial inflation and dark matter*, *Eur. Phys. J. C* **81** (2021) 877 [[2106.03950](#)].
- [26] M. Drees and Y. Xu, *Large field polynomial inflation: parameter space, predictions and (double) eternal nature*, *JCAP* **12** (2022) 005 [[2209.07545](#)].
- [27] R. Kallosh and A. Linde, *Universality Class in Conformal Inflation*, *JCAP* **07** (2013) 002 [[1306.5220](#)].
- [28] R. Kallosh, A. Linde and D. Roest, *Superconformal Inflationary α -Attractors*, *JHEP* **11** (2013) 198 [[1311.0472](#)].
- [29] K. Mukaida and M. Yamada, *Thermalization Process after Inflation and Effective Potential of Scalar Field*, *JCAP* **02** (2016) 003 [[1506.07661](#)].
- [30] M.A.G. Garcia and M.A. Amin, *Prethermalization production of dark matter*, *Phys. Rev. D* **98** (2018) 103504 [[1806.01865](#)].
- [31] D. Chowdhury and A. Hait, *Thermalization in the presence of a time-dependent dissipation and its impact on dark matter production*, *JHEP* **09** (2023) 085 [[2302.06654](#)].
- [32] M.A. Amin, M.P. Hertzberg, D.I. Kaiser and J. Karouby, *Nonperturbative Dynamics Of Reheating After Inflation: A Review*, *Int. J. Mod. Phys. D* **24** (2014) 1530003 [[1410.3808](#)].

- [33] M.A.G. Garcia, K. Kaneta, Y. Mambrini, K.A. Olive and S. Verner, *Freeze-in from preheating*, *JCAP* **03** (2022) 016 [[2109.13280](#)].
- [34] K.D. Lozanov and M.A. Amin, *Equation of State and Duration to Radiation Domination after Inflation*, *Phys. Rev. Lett.* **119** (2017) 061301 [[1608.01213](#)].
- [35] M.A.G. Garcia and M. Pierre, *Reheating after inflaton fragmentation*, *JCAP* **11** (2023) 004 [[2306.08038](#)].
- [36] M.A.G. Garcia, M. Gross, Y. Mambrini, K.A. Olive, M. Pierre and J.-H. Yoon, *Effects of fragmentation on post-inflationary reheating*, *JCAP* **12** (2023) 028 [[2308.16231](#)].
- [37] N. Bernal, J. Rubio and H. Veermäe, *UV Freeze-in in Starobinsky Inflation*, *JCAP* **10** (2020) 021 [[2006.02442](#)].
- [38] S. Clery, Y. Mambrini, K.A. Olive and S. Verner, *Gravitational portals in the early Universe*, *Phys. Rev. D* **105** (2022) 075005 [[2112.15214](#)].
- [39] M.R. Haque and D. Maity, *Gravitational reheating*, *Phys. Rev. D* **107** (2023) 043531 [[2201.02348](#)].
- [40] B. Barman, N. Bernal and J. Rubio, *Rescuing Gravitational-Reheating in Chaotic Inflation*, [2310.06039](#).
- [41] M.R. Haque, D. Maity and R. Mondal, *ν GR: Gravitational ν trino Reheating*, [2311.07684](#).
- [42] J.F. Dufaux, G.N. Felder, L. Kofman, M. Peloso and D. Podolsky, *Preheating with trilinear interactions: Tachyonic resonance*, *JCAP* **07** (2006) 006 [[hep-ph/0602144](#)].
- [43] D. Maity and P. Saha, *(P)reheating after minimal Plateau Inflation and constraints from CMB*, *JCAP* **07** (2019) 018 [[1811.11173](#)].
- [44] R.T. Co, Y. Mambrini and K.A. Olive, *Inflationary gravitational leptogenesis*, *Phys. Rev. D* **106** (2022) 075006 [[2205.01689](#)].
- [45] B. Barman, S. Cléry, R.T. Co, Y. Mambrini and K.A. Olive, *Gravity as a portal to reheating, leptogenesis and dark matter*, *JHEP* **12** (2022) 072 [[2210.05716](#)].
- [46] S. Clery, Y. Mambrini, K.A. Olive, A. Shkerin and S. Verner, *Gravitational portals with nonminimal couplings*, *Phys. Rev. D* **105** (2022) 095042 [[2203.02004](#)].
- [47] Y. Xu, *Constraining axion and ALP dark matter from misalignment during reheating*, *Phys. Rev. D* **108** (2023) 083536 [[2308.15322](#)].
- [48] G.F. Giudice, E.W. Kolb and A. Riotto, *Largest temperature of the radiation era and its cosmological implications*, *Phys. Rev. D* **64** (2001) 023508 [[hep-ph/0005123](#)].
- [49] PLANCK collaboration, *Planck 2018 results. VI. Cosmological parameters*, *Astron. Astrophys.* **641** (2020) A6 [[1807.06209](#)].
- [50] Y. Mambrini, K.A. Olive and J. Zheng, *Post-inflationary dark matter bremsstrahlung*, *JCAP* **10** (2022) 055 [[2208.05859](#)].
- [51] D. Hooper, G. Krnjaic, A.J. Long and S.D. McDermott, *Can the Inflaton Also Be a Weakly Interacting Massive Particle?*, *Phys. Rev. Lett.* **122** (2019) 091802 [[1807.03308](#)].
- [52] M.A.G. Garcia, Y. Mambrini, K.A. Olive and S. Verner, *On the Realization of WIMPflation*, *JCAP* **10** (2021) 061 [[2107.07472](#)].

- [53] BICEP, KECK collaboration, *Improved Constraints on Primordial Gravitational Waves using Planck, WMAP, and BICEP/Keck Observations through the 2018 Observing Season*, *Phys. Rev. Lett.* **127** (2021) 151301 [[2110.00483](#)].
- [54] N. Aggarwal et al., *Challenges and opportunities of gravitational-wave searches at MHz to GHz frequencies*, *Living Rev. Rel.* **24** (2021) 4 [[2011.12414](#)].
- [55] LISA collaboration, *Laser Interferometer Space Antenna*, [1702.00786](#).
- [56] M. Punturo et al., *The Einstein Telescope: A third-generation gravitational wave observatory*, *Class. Quant. Grav.* **27** (2010) 194002.
- [57] S. Hild et al., *Sensitivity Studies for Third-Generation Gravitational Wave Observatories*, *Class. Quant. Grav.* **28** (2011) 094013 [[1012.0908](#)].
- [58] B. Sathyaprakash et al., *Scientific Objectives of Einstein Telescope*, *Class. Quant. Grav.* **29** (2012) 124013 [[1206.0331](#)].
- [59] M. Maggiore et al., *Science Case for the Einstein Telescope*, *JCAP* **03** (2020) 050 [[1912.02622](#)].
- [60] J. Crowder and N.J. Cornish, *Beyond LISA: Exploring future gravitational wave missions*, *Phys. Rev. D* **72** (2005) 083005 [[gr-qc/0506015](#)].
- [61] V. Corbin and N.J. Cornish, *Detecting the cosmic gravitational wave background with the big bang observer*, *Class. Quant. Grav.* **23** (2006) 2435 [[gr-qc/0512039](#)].
- [62] G.M. Harry, P. Fritschel, D.A. Shaddock, W. Folkner and E.S. Phinney, *Laser interferometry for the big bang observer*, *Class. Quant. Grav.* **23** (2006) 4887.
- [63] N. Seto, S. Kawamura and T. Nakamura, *Possibility of direct measurement of the acceleration of the universe using 0.1-Hz band laser interferometer gravitational wave antenna in space*, *Phys. Rev. Lett.* **87** (2001) 221103 [[astro-ph/0108011](#)].
- [64] H. Kudoh, A. Taruya, T. Hiramatsu and Y. Himemoto, *Detecting a gravitational-wave background with next-generation space interferometers*, *Phys. Rev. D* **73** (2006) 064006 [[gr-qc/0511145](#)].
- [65] F.-Y. Li, M.-X. Tang and D.-P. Shi, *Electromagnetic response of a Gaussian beam to high frequency relic gravitational waves in quintessential inflationary models*, *Phys. Rev. D* **67** (2003) 104008 [[gr-qc/0306092](#)].
- [66] A. Berlin, D. Blas, R. Tito D’Agnolo, S.A.R. Ellis, R. Harnik, Y. Kahn et al., *Detecting high-frequency gravitational waves with microwave cavities*, *Phys. Rev. D* **105** (2022) 116011 [[2112.11465](#)].
- [67] A. Berlin, D. Blas, R. Tito D’Agnolo, S.A.R. Ellis, R. Harnik, Y. Kahn et al., *Electromagnetic cavities as mechanical bars for gravitational waves*, *Phys. Rev. D* **108** (2023) 084058 [[2303.01518](#)].
- [68] N. Herman, L. Lehoucq and A. Fúza, *Electromagnetic antennas for the resonant detection of the stochastic gravitational wave background*, *Phys. Rev. D* **108** (2023) 124009 [[2203.15668](#)].
- [69] E. Armengaud et al., *Conceptual Design of the International Axion Observatory (IAXO)*, *JINST* **9** (2014) T05002 [[1401.3233](#)].
- [70] IAXO collaboration, *Physics potential of the International Axion Observatory (IAXO)*, *JCAP* **06** (2019) 047 [[1904.09155](#)].

- [71] C. Caprini and D.G. Figueroa, *Cosmological Backgrounds of Gravitational Waves*, *Class. Quant. Grav.* **35** (2018) 163001 [[1801.04268](#)].
- [72] CORE collaboration, *COrE (Cosmic Origins Explorer) A White Paper*, [1102.2181](#).
- [73] EUCLID collaboration, *Euclid Definition Study Report*, [1110.3193](#).
- [74] I. Ben-Dayan, B. Keating, D. Leon and I. Wolfson, *Constraints on scalar and tensor spectra from N_{eff}* , *JCAP* **06** (2019) 007 [[1903.11843](#)].
- [75] M. Maggiore, *Gravitational wave experiments and early universe cosmology*, *Phys. Rept.* **331** (2000) 283 [[gr-qc/9909001](#)].